



---

Adarakatti, PS, Mahanthappa, M, Hughes, JP, Rowley-Neale, SJ ORCID logoORCID: <https://orcid.org/0000-0002-3741-4050>, Smith, GC, S, A and Banks, CE ORCID logoORCID: <https://orcid.org/0000-0002-0756-9764> (2019) MoS<sub>2</sub>-graphene-CuNi<sub>2</sub>S<sub>4</sub> nanocomposite an efficient electrocatalyst for the hydrogen evolution reaction. International Journal of Hydrogen Energy, 44 (31). pp. 16069-16078. ISSN 0360-3199

---

**Downloaded from:** <https://e-space.mmu.ac.uk/624355/>

**Version:** Accepted Version

**Publisher:** Elsevier

**DOI:** <https://doi.org/10.1016/j.ijhydene.2019.05.004>

**Usage rights:** Creative Commons: Attribution-Noncommercial-No Derivative Works 4.0

Please cite the published version

<https://e-space.mmu.ac.uk>

# MoS<sub>2</sub>-graphene-CuNi<sub>2</sub>S<sub>4</sub> Nanocomposite an Efficient Electrocatalyst for the Hydrogen Evolution Reaction

Prashanth Shivappa Adarakatti<sup>1†</sup>, Mallappa Mahanthappa<sup>2†</sup>, Jack P. Hughes,<sup>3</sup> Samuel J. Rowley-Neale,<sup>3,4†</sup> Graham C. Smith,<sup>5</sup> Ashoka S,<sup>6</sup> and Craig E. Banks<sup>4,5\*</sup>

<sup>1</sup>: *Solid State and Structural Chemistry Unit, Indian Institute of Science, Bengaluru - 560012, India*

<sup>2</sup>: *Department of Chemistry, School of Chemical Sciences, REVA University, Bengaluru - 560064, India*

<sup>3</sup>: *Faculty of Science and Engineering, School of Science and the Environment, Division of Chemistry and Environmental Science, Manchester Metropolitan University, Chester Street, Manchester M1 5GD, UK.*

<sup>4</sup>: *Manchester Fuel Cell Innovation Centre, Manchester Metropolitan University, Chester Street, Manchester M1 5GD, UK.*

<sup>5</sup>: *Faculty of Science and Engineering, Department of Natural Sciences, University of Chester, Thornton Science Park, Pool Lane, Ince, Chester CH2 4NU, UK*

<sup>6</sup>: *Department of Chemistry, School of Engineering, Dayananda Sagar University, Bengaluru-560068, India*

\*To whom correspondence should be addressed.

† These authors contributed equally

Email: [c.banks@mmu.ac.uk](mailto:c.banks@mmu.ac.uk); Tel: ++(0)1612471196; Fax: ++(0)1612476831

Website: [www.craigbanksresearch.com](http://www.craigbanksresearch.com)

## 1. Abstract

We present a facile methodology for the synthesis of a novel 2D-MoS<sub>2</sub>, graphene and CuNi<sub>2</sub>S<sub>4</sub> (MoS<sub>2</sub>-g-CuNi<sub>2</sub>S<sub>4</sub>) nanocomposite that displays highly efficient electrocatalytic activity towards the production of hydrogen. The intrinsic hydrogen evolution reaction (HER) activity of MoS<sub>2</sub> nanosheets was significantly enhanced by increasing the affinity of the active edge sites towards H<sup>+</sup> adsorption using transition metal (Cu and Ni<sub>2</sub>) dopants, whilst also increasing the edge sites exposure by anchoring them to a graphene framework. Detailed XPS analysis reveals a higher percentage of surface exposed S at 17.04%, of which 48.83% is metal bonded S (sulfide). The resultant MoS<sub>2</sub>-g-CuNi<sub>2</sub>S<sub>4</sub> nanocomposites are immobilized upon screen-printed electrodes (SPEs) and exhibit a HER onset potential and Tafel slope value of – 0.05 V (*vs.* RHE) and 29.3 mV dec<sup>-1</sup>, respectively. These values are close to that of the polycrystalline Pt electrode (near zero potential (*vs.* RHE) and 21.0 mV dec<sup>-1</sup>, respectively) and enhanced over bare/unmodified SPE (– 0.43 V (*vs.* RHE) and 149.1 mV dec<sup>-1</sup>, respectively). Given the efficient, HER activity displayed by the novel MoS<sub>2</sub>-g-CuNi<sub>2</sub>S<sub>4</sub>/SPE electrochemical platform and the comparatively low associated cost of production for this nanocomposite, it has potential to be a cost-effective alternative to Pt within electrolyser technologies.

**Keywords:** Molybdenum disulfide (MoS<sub>2</sub>), graphene, Hydrogen Evolution Reaction, Energy storage

## 2. Introduction

A plethora of emergent low polluting energy generation technologies rely upon hydrogen gas as a fuel source[37], which has created an impetus for clean hydrogen generation techniques to be developed. A prominent method for clean hydrogen generation is the Hydrogen Evolution Reaction (HER); ( $2\text{H}^+ + 2\text{e}^- \rightarrow \text{H}_2$ ), which is the cathodic reaction within an electrolyser.[1] The power necessary to operate an electrolyser could feasibly be drawn from renewable sources, making it a “cleaner” fuel source compared to its fossil fuel (FF) counterparts.[32] A limiting factor to the ubiquitous use of electrolyzers to generate hydrogen is the requirement for expensive platinum (Pt) as a catalyst for the HER.[13, 18, 31] Much of the research dedicated to finding an alternative to Pt has focused upon the di-chalcogenides, particularly MoS<sub>2</sub> based materials (see Table 1),[31] as 2D-MoS<sub>2</sub> nanosheets have been shown to be effective at lowering the HER onset potential and increasing the achievable current density, whilst typically being composed of significantly cheaper and more earth abundant elements.[7, 17, 19] For example a study by Ruiz *et al.*[35] utilized a chemical vapor deposition (CVD) technique to grow vertically aligned MoS<sub>2</sub> on a gold foil and demonstrated how the optimized (prepared at 600°C) MoS<sub>2</sub> film, when used as an electrode, achieved a current density of 10 mA cm<sup>-2</sup> by -0.355 V (*vs.* saturated calomel electrode (SCE)). Whilst being *ca.* -0.250 V (*vs.* SCE) more electronegative than the optimal value of Pt, it was significantly less electronegative than the values reported by Rowley-Neale *et al.*[31] for unmodified traditional carbon based electrodes (boron doped diamond, edge-plane pyrolytic graphite, glassy carbon and screen-printed electrodes (SPE)).

There are a wide variety of studies within the literature, which demonstrate the capability of a MoS<sub>2</sub> based material to act as an efficient electrocatalyst towards the HER, however few reports show any form of catalyst that can display equivalent HER activity to Pt based electrocatalysts. In order to narrow the potential gap between the HER onset potentials of MoS<sub>2</sub> and Pt based catalysts, numerous studies have utilized MoS<sub>2</sub> nanosheets as a dopant framework in order to fabricate electrocatalysts that show more comparable HER activity to Pt. One such study by Shi *et al.*[38] found that Zinc (Zn) doped MoS<sub>2</sub> (Zn-MoS<sub>2</sub>) when drop-cast onto a GC electrode exhibited greater HER catalysis than undoped MoS<sub>2</sub>, with a HER onset potential of -0.13 V (*vs.* reversible hydrogen electrode (RHE)) and a Tafel slope of 51 mV dec<sup>-1</sup> compared to -1.4 V (*vs.* RHE) and 101 mV dec<sup>-1</sup> for undoped MoS<sub>2</sub> nanosheets. Shi and coworkers.[38] attributed the increased HER activity

to a synergistic electron (energy level matching) and morphological effect (increase in the number of exposed active edge sites) between the Zn and the MoS<sub>2</sub> nanosheets.

HER catalysis is thought to predominately occur at the MoS<sub>2</sub> nanosheets edge sites, in particular the exposed Sulfur atoms, which have an affinity towards H<sup>+</sup> adsorption due to a density functional theory predicting a binding energy of +0.08 eV.[19] In contrast to this, the basal sites are relatively inert and show little catalytic activity,[47] consequently the bulk of the material can be considered electrocatalytically inert.[6] Efforts to maximize the ratio of edge sites to basal sites of a given MoS<sub>2</sub> based material would therefore yield a more effective HER catalyst. Previous studies have shown that hybridizing an electrocatalyst with a graphitic material (*e.g.* reduced graphene oxide) offers a beneficial morphology (an increased number of exposed active sites) leading to increased catalysis.[21] Hybridization in this manner has the additional benefit of improving charge transfer and conductivity for the entire system and notably, the electrocatalytic sites.[10]

Given the above, there are two major factors that should be considered in research focused on optimizing HER catalysis of MoS<sub>2</sub> containing materials. The first being: increasing the affinity of active sites towards H<sup>+</sup> adsorption and thus their ability to catalyze the HER. Secondly: maximizing the ratio of exposed active edge sites to inert basal sites, which will increase the density of sites enabling catalysis. In order to tackle both of these challenges we present a novel methodology for doping MoS<sub>2</sub> with transition metals (Cu and Ni) in order to increase the electron density at the electrocatalytically active edge sites and therefore improve their HER activity, whilst increasing the exposure of these sites by anchoring them to a graphene framework. The novel MoS<sub>2</sub>-graphene-CuNi<sub>2</sub>S<sub>4</sub> (MoS<sub>2</sub>-g-CuNi<sub>2</sub>S<sub>4</sub>) nanocomposite is electrically wired *via* immobilization upon SPEs and experimentally explored towards the HER where it exhibits highly efficient HER catalysis.

### 3. Experimental

#### 3.1. Chemicals

The MoS<sub>2</sub>-g-CuNi<sub>2</sub>S<sub>4</sub> nanocomposite precursors utilized in this study were, Cu(NO<sub>3</sub>)<sub>2</sub>.6H<sub>2</sub>O, Ni(NO<sub>3</sub>)<sub>2</sub>.6H<sub>2</sub>O, thiourea, MoS<sub>2</sub>, graphite powder (30 μm) and polyvinylpyrrolidone. All of precursors were purchased from Sigma Aldrich, Merck and Sd-fine chemical PVT Ltd, respectively and used without further purification. All solutions were prepared with doubly distilled water (18.2 MΩ cm) and were vigorously degassed prior to electrochemical measurements with high purity, oxygen free, nitrogen. All experiments were performed in 0.5 M H<sub>2</sub>SO<sub>4</sub> in order to replicate the conditions found within an acidic proton exchange membrane fuel cell (PEMFC).[34]

#### 3.2. Electrochemical Measurements

Electrochemical measurements were studied using CH-Electrochemical analyzer model CHI 6039E (USA). Measurements were carried out using a typical three electrode system with a nickel wire counter and a reversible hydrogen electrode (RHE) reference electrode. The working electrodes are screen-printed graphite macro electrodes (SPEs) comprising a 3.1 mm diameter working area. The SPEs were fabricated in-house with the appropriate stencils using a DEK 248 screen-printing machine (DEK, Weymouth, U.K.).[9] The fabrication of the SPEs has been extensively described in previous publications,[34] however it is repeated within the supporting information for clarity.

#### 3.3. Synthesis of MoS<sub>2</sub>-g-CuNi<sub>2</sub>S<sub>4</sub> nanocomposite

The MoS<sub>2</sub>-g-CuNi<sub>2</sub>S<sub>4</sub> nanocomposites were synthesized by the following protocol. In brief, 120 mg of graphite (<20 μm) and MoS<sub>2</sub> powder were mixed into a solution containing a 1:1 mixture of water/isopropanol. This solution was then ultra-sonicated for 3 hrs. Following this, 1 mM of Cu(NO<sub>3</sub>)<sub>2</sub>.6H<sub>2</sub>O, 2 mM Ni(NO<sub>3</sub>)<sub>2</sub>.6H<sub>2</sub>O, PVP and thiourea were added to 12.5 mL of the graphene/MoS<sub>2</sub> solution at a concentration of 1, 2, 1 and 9 mM, respectively. Next, 1 mL of ammonia was added drop wise to the solution under continuous stirring. The solution mixture was then transferred into a Teflon lined autoclave, sealed and heated, at 180 °C, for 24 h. The obtained black solid product was filtered, washed with water and ethanol several times then left to in a hot

air oven, at 80 °C, for 12 h. For comparative purposes CuNi<sub>2</sub>S<sub>4</sub>, g-CuNi<sub>2</sub>S<sub>4</sub> and MoS<sub>2</sub>-CuNi<sub>2</sub>S<sub>4</sub> were fabricated in the same manner and electrochemically explored towards the HER.

### ***3.4. Instrumentation***

The phase transition, purity and crystal structure of the synthesized compounds were analyzed by a PANalytical X'pert PRO powder X-ray powder diffractometer (XRD) equipped with Ni-filtrated Cu K $\alpha$  radiation (40 kV, 200 mA). The composition and functional groups present in the as prepared catalyst was monitored by Agilent carry-630 Fourier transform infrared (FT-IR) spectroscopy over the range of 400-4000 cm<sup>-1</sup>. Raman Spectroscopy was performed using a 'Renishaw InVia' spectrometer equipped with a confocal microscope ( $\times 50$  objective) and an argon laser (514.3 nm excitation). Measurements were performed at a very low laser power level (0.8 mW) to avoid any heating effects. The optical absorbance spectra of as prepared HER catalyst was monitored by UV-visible absorption spectroscopy (UV-1800, Shimadzu, Japan). The morphology, composition, size and crystallinity of the as prepared HER catalyst was analyzed by scanning electron microscope (SEM) using a JEOL JSM-5600LV model SEM. Transmission electron microscopy (TEM) images were obtained using a 200 kV primary beam under conventional bright-field conditions with an energy dispersive X-ray microanalysis (EDX) package. The MoS<sub>2</sub>-g-CuNi<sub>2</sub>S<sub>4</sub> sample was dispersed onto a holey-carbon film supported on a 300 mesh Cu TEM grid. X-ray photoelectron (XPS) analysis of the samples was performed using a bespoke ultra-high vacuum system fitted with a Specs GmbH Focus 500 monochromated Al K $\alpha$  X-ray source, Specs GmbH Phoibos 150 mm mean radius hemispherical analyser with 9-channeltron detection, and a Specs GmbH FG20 charge neutralising electron gun. The Al monochromator source was used to generate a survey scan and higher resolution scans over C 1s, O 1s, Cu 2p, Ni 2p, N 1s, S 2p and, where detected, Mo 3d photoelectron lines. A representative area approximately 1.4 mm in diameter over the center of each sample was analysed.

### ***3.5. Electrode preparation***

Following the synthesis of the nanocomposites, their HER activity was electrochemically explored. This was done by dispersing 5 mg of the catalyst and 5 wt% nafion into a solution of water and ethanol, the solution was ultra-sonicated for 30 min to ensure it was homogenous. 5  $\mu$ L

of this suspension was then drop-caste (where an aliquot of the given solution is deposited onto the working area of an SPE, using a manual micro-pipette). This resulted in a surface coverage of *ca.*  $0.3 \text{ mg cm}^{-2}$  MoS<sub>2</sub>-g-CuNi<sub>2</sub>S<sub>4</sub>. The electrode was then air dried for 30 mins to ensure evaporation of the water and ethanol. The prepared electrode was then ready for use.



## 4. Results and Discussion

### 4.1. Physicochemical characterization of the nanocomposites

A thorough physicochemical analysis of the novel synthesized MoS<sub>2</sub>-g-CuNi<sub>2</sub>S<sub>4</sub> nanocomposite, was performed using FT-IR, Raman spectroscopy, SEM, TEM, TGA, EDX, XRD and XPS.

TEM imaging of the MoS<sub>2</sub>-g-CuNi<sub>2</sub>S<sub>4</sub> nanocomposite is shown in Figure 1 showing that the MoS<sub>2</sub>-g-CuNi<sub>2</sub>S<sub>4</sub> nanocomposite had an average diameter of *ca.* 50 nm, however there are signs of agglomeration of the new particles. Note that Figure 1(B) has five separate sites identified which are the locations of elemental composition analysis *via* EDX, the results of which are prescribed within in Table S1. Note that the presence of all the expected elementals, and there is a higher than expected percentage of Cu observed, which is likely a result of the use of a Cu supporting grid. EDX mapping of a MoS<sub>2</sub>-g-CuNi<sub>2</sub>S<sub>4</sub> flake (see ESI Figure S1) showed uniform distribution S, Cu, Ni, Mo and O upon the flakes surface. The FTIR spectrum of the MoS<sub>2</sub>-g-CuNi<sub>2</sub>S<sub>4</sub> nanocomposite is given in Figure 2(A). The majority of peaks between 1000-4000 cm<sup>-1</sup> can be ascribed to graphitic components, for example the peaks at 1609 and 2911 cm<sup>-1</sup> are characteristic of sp<sup>2</sup> hybridized carbon and hydroxyl groups, respectively.[40] Note the peak at 3434 cm<sup>-1</sup> is the characteristic band of O-H.[50] The weak observable peak at 479 is likely due to Mo-S vibration.[26] Raman spectroscopy was also performed on the MoS<sub>2</sub>-g-CuNi<sub>2</sub>S<sub>4</sub> with the obtained spectrum being shown in Figure 2(B). Vibrational bands (VB) at *ca.* 378 and 403 cm<sup>-1</sup>, which correspond to the E<sub>2g</sub><sup>1</sup> and A<sub>1g</sub> of MoS<sub>2</sub>, can be observed.[20] Additionally VBs at *ca.* 1360 and 1578 cm<sup>-1</sup> are observed, these correspond to the D and G bands of a graphitic material.[4, 29] Finally, the presence of a peak at *ca.* 2713 cm<sup>-1</sup> (2D band) is also characteristic of graphitic materials,[4, 8] thus confirming the presence of high quality few layer graphene and MoS<sub>2</sub>. [16, 28] The XRD profile of the MoS<sub>2</sub>-g-CuNi<sub>2</sub>S<sub>4</sub> nanocomposite is shown in Figure 2(D). Except for the indexed MoS<sub>2</sub> peaks (corresponding to JCPDS No. 37-1492), all of the other diffraction peaks can be ascribed to the cubic phase of CuNi<sub>2</sub>S<sub>4</sub> (JCPDS No. 24-334). For instance, the typical diffraction peaks of (311), (400), (511), and (440) diffraction planes can be clearly indexed at 31.4°, 38.2°, 50.1°, and 55.1°, respectively. No obvious peaks from other phases such as CuS, NiS, or organic compounds related to the precursors were detected. Furthermore, graphene/graphite peak (002) at 26.5°,[28] in the XRD patterns as well as the characteristic (002) peak for MoS<sub>2</sub> at 14.2°.[15] It was important to determine the elemental composition of each of the nanocomposites, therefore XPS analysis was performed on the samples.

A typical survey spectra of the MoS<sub>2</sub>-g-CuNi<sub>2</sub>S<sub>4</sub> is shown in Figure 2(C), where all the expected elements can be observed as well as low levels of N and Si (the presence of N is likely due to atmospheric contamination, whilst the Si can be attributed to the Si containing adhesive tape used to fix the samples during analysis). The full elemental composition of each composite material is shown within Table 2. Table 3 gives the results of the quantification analysis of all the synthesized nanocomposites and ESI Figure S2 displays high resolution XPS spectra of the Mo, S, C, O, Cu and Ni components for the MoS<sub>2</sub>-g-CuNi<sub>2</sub>S<sub>4</sub> nanocomposite. Note that further XPS analysis is described later within the manuscript in order to provide insights into the substantial HER activity observed by the MoS<sub>2</sub>-g-CuNi<sub>2</sub>S<sub>4</sub>. Lastly, thermogravimetric analysis assessed the thermal stability of the MoS<sub>2</sub>-g-CuNi<sub>2</sub>S<sub>4</sub>. It is clear from inspection of ESI Figure 3 that the nanocomposite was stable until *ca.* 200°C after which the MoS<sub>2</sub>-CuNi<sub>2</sub>S<sub>4</sub> exhibited a rapid and uniform decomposition to *ca.* 75% by 900°C. The average working temperature of a proton exchange membrane electrolyser is between 50-80 °C,[11] so MoS<sub>2</sub>-g-CuNi<sub>2</sub>S<sub>4</sub> could maintain its composition within an operating electrolyser. Given the thorough physicochemical analysis given above the MoS<sub>2</sub>-g-CuNi<sub>2</sub>S<sub>4</sub> nanocomposite is shown to be of high purity and crystallinity.

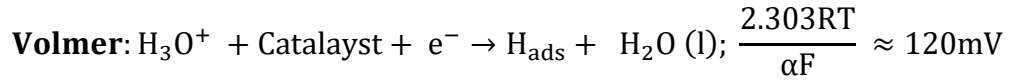
#### ***4.2. Application of the MoS<sub>2</sub>-g-CuNi<sub>2</sub>S<sub>4</sub>/SPEs towards the HER***

Initially it was important to benchmark the electrochemical behavior of a bare/unmodified SPE and a polycrystalline platinum (Pt) electrode towards the HER in 0.5 M H<sub>2</sub>SO<sub>4</sub>. Figure 3(A) shows the linear sweep voltammetry (LSV) obtained for a bare/unmodified SPE and Pt electrode as well as for the CuNi<sub>2</sub>S<sub>4</sub>/SPE, g-CuNi<sub>2</sub>S<sub>4</sub>/SPE, MoS<sub>2</sub>-CuNi<sub>2</sub>S<sub>4</sub>/SPE and MoS<sub>2</sub>-g-CuNi<sub>2</sub>S<sub>4</sub>/SPEs. The bare/unmodified SPE had an onset potential of – 0.43 V (*vs.* RHE), as expected this is far more electronegative than the optimal HER onset potential for Pt. Note that within this study the HER onset potential is determined as the potential when the current deviates from the background current by 25 μA cm<sup>-2</sup>. From inspection of Figure 3(A) it is clear that upon immobilization of all of the nanocomposites onto an SPE there is a decrease in the electronegativity of the HER onset potential, with the CuNi<sub>2</sub>S<sub>4</sub>/SPE, g-CuNi<sub>2</sub>S<sub>4</sub>/SPE, MoS<sub>2</sub>-CuNi<sub>2</sub>S<sub>4</sub>/SPE and MoS<sub>2</sub>-g-CuNi<sub>2</sub>S<sub>4</sub>/SPE exhibiting HER onset potentials of – 0.41, – 0.15, – 0.13 and – 0.05 V (*vs.* RHE), respectively. It is also worth noting there is a corresponding increase in the achievable current densities with the MoS<sub>2</sub>-g-CuNi<sub>2</sub>S<sub>4</sub>/SPEs reaching 10 mA cm<sup>-2</sup> by – 0.12 V (*vs.* RHE). In comparison of the nanocomposites synthesized, the MoS<sub>2</sub>-g-CuNi<sub>2</sub>S<sub>4</sub>/SPE displays the most optimal HER activity

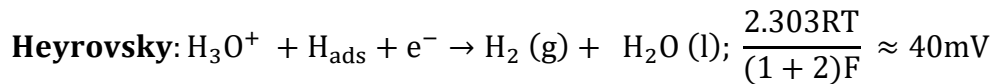
with a HER onset potential close to that of Pt. This is likely a result of MoS<sub>2</sub>-g-CuNi<sub>2</sub>S<sub>4</sub> having the largest number of exposed active edge sites for H<sup>+</sup> adsorption as a result of the graphene acting as a framework for optimal exhibition of the sulfur edge sites of MoS<sub>2</sub> and CuNi<sub>2</sub>S<sub>4</sub> in addition to the electrocatalytically active functional moieties in graphene. Additionally, the graphene acted to increase the electroconductivity, whilst the interface in MoS<sub>2</sub>-g- CuNi<sub>2</sub>S<sub>4</sub> facilitates the electron transfer during electrocatalysis.

### 4.3. Tafel Analysis

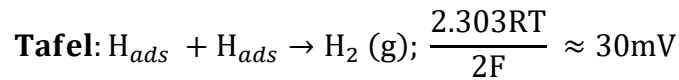
In order to determine whether the increased HER activity observed from an SPE post nanocomposite immobilization was as a result of the catalyst enabling a change in the reaction mechanism, Tafel analysis was performed. The activity of a HER catalyst is related to the kinetic barrier of the rate-determining hydrogen evolution pathway. According to the literature, HER mechanism involves three possible rate limiting steps, those being: (i) initial H<sup>+</sup> adsorption step, known as the Volmer step,



(ii) Volmer- Heyrosky discharge step:



(iii) Volmer-Tafel discharge step :



where the transfer coefficient ( $\alpha$ ) is 0.5,  $F$  is the Faraday constant,  $R$  is the universal gas constant and  $T$  is the temperature at which the electrochemical experiment was performed (298 K). Tafel analysis was performed on the Faradaic section of the LSVs shown in Figure 3(A) with the resultant Tafel slopes being given in Figure 3(B). The determined Tafel slopes for the bare/unmodified SPE and Pt electrodes were 149.1 and 21.0 mV dec<sup>-1</sup>, respectively, these values correspond to those reported in previous literature. The determined Tafel values suggest that the rate limiting step of the HER mechanism on a bare/unmodified SPE is the Volmer step whilst a Pt electrode allows the HER to occur *via* the desirable Volmer-Tafel mechanism. The Tafel slope

values obtained for the CuNi<sub>2</sub>S<sub>4</sub>/SPE, g-CuNi<sub>2</sub>S<sub>4</sub>/SPE, MoS<sub>2</sub>-CuNi<sub>2</sub>S<sub>4</sub>/SPE and MoS<sub>2</sub>-g-CuNi<sub>2</sub>S<sub>4</sub>/SPEs were 147.3, 111.8, 44.7 and 29.3 mV dec<sup>-1</sup> respectively. Interpretation of these Tafel values, reveals that for the CuNi<sub>2</sub>S<sub>4</sub>/SPE and g-CuNi<sub>2</sub>S<sub>4</sub>/SPE there is not an alteration in the reaction mechanism with the Volmer adsorption step still being the rate limiting step. However, for the MoS<sub>2</sub>-CuNi<sub>2</sub>S<sub>4</sub>/SPE and MoS<sub>2</sub>-g-CuNi<sub>2</sub>S<sub>4</sub>/SPEs there is a significant increase in the current density resulting in the Tafel discharge step becoming the rate limiting step. The smallest Tafel value was recorded for the MoS<sub>2</sub>-g-CuNi<sub>2</sub>S<sub>4</sub>/SPE, this suggests that MoS<sub>2</sub>-g-CuNi<sub>2</sub>S<sub>4</sub> substantially enhances the HER capability of the SPE platform to close to that of a Pt electrode. The data presented above clearly shows that hybridization of MoS<sub>2</sub> with graphene and CuNi<sub>2</sub>S<sub>4</sub> significantly improves HER catalysis. The literature suggests that it is the exposed sulfur atoms located at the MoS<sub>2</sub> nanosheets edge sites that produce HER activity, it was therefore vital that we investigate the chemical changes responsible for the reported increase in catalysis. A detailed quantitative XPS analysis of the S components for each of the nanocomposites was performed. The obtained high resolution S 2p spectra (See ESI Figure S2) were complex in shape, exhibiting good evidence for 4 separate chemical environments. S 2p peaks were fitted with multiple sets of 2p<sub>3/2</sub>-2p<sub>1/2</sub> doublets. In each case, the two components of the doublet had to be constrained to the same width and line shape, the area ratio is constrained so that the 2p<sub>1/2</sub> component is 50% of the intensity of the 2p<sub>3/2</sub> component (as expected from orbital occupancies), and the two components are constrained to be separated by 1.13 eV. The 4 separate chemical environments for S were: Metal-bonded S *e.g.* metal sulfide bonds such as Cu-S, Ni-S, Mo-S, typically 161 – 162 eV, Metal bonded to organic S, typically 162.5 – 163 eV, organic (carbon bonded) sulfur, typically 164.4 – 164.6 eV, and oxidized S *e.g.* as sulfate, typically 168.4 – 168.5 eV. The relative percentage quantity of each of these components with the four nanocomposites is summarized in Table 3. It is evident that there is a strong positive correlation between atomic percentage of S (especially metal bonded S) and electrocatalytic activity towards the HER for the MoS<sub>2</sub>-g-CuNi<sub>2</sub>S<sub>4</sub>, MoS<sub>2</sub>- CuNi<sub>2</sub>S<sub>4</sub> and g-CuNi<sub>2</sub>S<sub>4</sub>. As shown by analysis of the MoS<sub>2</sub>-g-CuNi<sub>2</sub>S<sub>4</sub>, which displayed the greatest HER catalysis and had the highest atomic percentage of S at 17.04%, of which 48.83% was metal bonded S (*the highest percentage recorded for any of the nanocomposites*). Note that CuNi<sub>2</sub>S<sub>4</sub> has the highest atomic percentage of S of all four nanocomposites and a higher % of metal bonded S than MoS<sub>2</sub>- CuNi<sub>2</sub>S<sub>4</sub> or g-CuNi<sub>2</sub>S<sub>4</sub>, however it displays the least amount of HER catalytic activity. We summarize this to the lack of Mo, and therefore the lack of Mo-S sulfides, within the CuNi<sub>2</sub>S<sub>4</sub>.

So whilst there is a relatively high % of metal-S bonds these are likely Cu-S and Ni-S, therefore suggesting that the S present is not in a chemical environment complimentary to HER catalysis.

The as prepared materials  $\text{CuNi}_2\text{S}_4$ ,  $\text{g-CuNi}_2\text{S}_4$ ,  $\text{MoS}_2\text{-CuNi}_2\text{S}_4$  and  $\text{MoS}_2\text{-g-CuNi}_2\text{S}_4$  were further examined using electrochemical impedance spectroscopy (EIS) in order to determine the impedance of the interface system. EIS is a useful technique to characterize interface reactions and electrode kinetics in HER. ESI Figure S4 shows the Nyquist plots recorded for all of the nanocomposite modified SPEs using an overpotential of 150 mV (vs. RHE). The  $\text{MoS}_2\text{-g-CuNi}_2\text{S}_4$  exhibited the smallest  $R_{ct}$  at 10.08  $\text{k}\Omega$  compared to 44.35, 39.27  $\text{k}\Omega$  and 112.0  $\text{k}\Omega$  for the  $\text{CuNi}_2\text{S}_4$ ,  $\text{g-CuNi}_2\text{S}_4$  and  $\text{MoS}_2\text{-CuNi}_2\text{S}_4$ , respectively. The EIS data presented above supports the prior inference that  $\text{MoS}_2\text{-g-CuNi}_2\text{S}_4$  is the most effective electrocatalyst for the HER as it displayed the fastest rate of reaction. Lastly it was essential to assess the stability, of the  $\text{MoS}_2\text{-g-CuNi}_2\text{S}_4$ , at catalyzing the HER, as longevity and durability are important considerations if catalyst is to be implemented in an industrial application.[23, 39, 44] The stability of the  $\text{MoS}_2\text{-g-CuNi}_2\text{S}_4/\text{SPEs}$  towards HER has been tested by performing 1000 repeat cycling voltammograms (See Figure 3(C)). A slight decrease in catalytic activity of  $\text{MoS}_2\text{-g-CuNi}_2\text{S}_4/\text{SPE}$  is observed over the course of the 1000 scans, with the current density at  $-0.10$  V decreasing from  $-134$   $\mu\text{A}$  for the first scan to  $98$   $\mu\text{A}$  for the 1000<sup>th</sup> scan. The observed decrease in HER catalysis over for the course of 1000 CVs is likely a result of the  $\text{MoS}_2\text{-g-CuNi}_2\text{S}_4$  delaminating from the supporting SPEs surface due to hydrogen bubbling from the surface as the HER occurs.[3]

## 5. Conclusions

The synthesis of a novel MoS<sub>2</sub>-g-CuNi<sub>2</sub>S<sub>4</sub> nanocomposite that displays remarkable HER catalysis upon immobilization to a SPE, has been reported. The intrinsic HER activity of MoS<sub>2</sub> was improved by increasing the affinity of the active edge sites, of the MoS<sub>2</sub> nanosheets, for H<sup>+</sup> adsorption using transition metal (Cu and Ni) dopants, whilst also increasing the edge sites exposure by anchoring them to a graphene framework. Through a detailed XPS analysis, we demonstrated that the synthesis process, in particular hybridizing the MoS<sub>2</sub> with graphene, increases the percentage of electrocatalytic surface exposed S as well as the proportion of metal bonded S from 15.95% and 40.02%, respectively for the MoS<sub>2</sub>-CuNi<sub>2</sub>S<sub>4</sub> nanocomposite to 17.04% and 48.83%, respectively for the MoS<sub>2</sub>-g-CuNi<sub>2</sub>S<sub>4</sub> nanocomposite. The optimized MoS<sub>2</sub>-g-CuNi<sub>2</sub>S<sub>4</sub> electrocatalyst when immobilized upon SPEs display near Pt HER activity with a HER onset potential and Tafel slope value of  $-0.05$  V (*vs.* RHE) and  $29.3$  mV dec<sup>-1</sup>, respectively. These values are far greater than those of a bare/unmodified SPE ( $-0.43$  V (*vs.* RHE) and  $149.1$  mV dec<sup>-1</sup>), and the equivalent masses of the other synthesized nanocomposites upon an SPE ((CuNi<sub>2</sub>S ( $-0.41$  V (*vs.* RHE) and  $147.3$  mV dec<sup>-1</sup>), g-CuNi<sub>2</sub>S<sub>4</sub> ( $-0.15$  V (*vs.* RHE) and  $111.8$  mV dec<sup>-1</sup>) and MoS<sub>2</sub>-CuNi<sub>2</sub>S<sub>4</sub> ( $-0.13$  V (*vs.* RHE) and  $44.7$  mV dec<sup>-1</sup>)). We have provided insights into the synthesis of a novel HER catalyst (MoS<sub>2</sub>-g-CuNi<sub>2</sub>S<sub>4</sub>), which exhibits a near Pt electrocatalytic activity towards the HER. Clearly MoS<sub>2</sub>-g-CuNi<sub>2</sub>S<sub>4</sub> has the potential to act as a cost effective alternative to Pt, when utilized as the cathodic electrocatalyst implemented within the triple phase boundary of commercial PEM electrolyzers.

## **Acknowledgements**

Funding from the Engineering and Physical Sciences Research Council (Reference: Grant Ref. EP/P007767/1) and the Supergen program. The Manchester Fuel Cell Innovation Centre is funded by the European Regional Development Fund. Ashoka S greatly thanks Science and Engineering Research Board (SERB, Project No. ECR/2017/000743) Government of India, for financial support.

**Table 1.** Comparison Table showing the HER activity of MoS<sub>2</sub> and MoS<sub>2</sub> containing compounds.

Catalyst	Supporting Electrode	Loading	Deposition Technique	Electrolyte	HER onset (V)	Tafel Slope (mV dec <sup>-1</sup> )	Reference
CD/MoS <sub>2</sub>	GC	—	Drop- cast	0.5 M H <sub>2</sub> SO <sub>4</sub>	<i>ca.</i> − 0.5 (vs. RHE)	22	[5]
P-doped MoS <sub>2</sub>	GC	0.32 mg cm <sup>-2</sup>	Drop- cast	0.5 M H <sub>2</sub> SO <sub>4</sub>	− 0.015 (vs. RHE)	34	[25]
MoS <sub>2</sub> -Ni <sub>3</sub> S <sub>2</sub> H	NF	—	Chemical synthesis	1.0 M KOH	− 0.037 (vs. RHE)	61	[46]
MoS <sub>2</sub> /C*	SPE	252.80 μg cm <sup>-2</sup>	Drop- cast	0.5 M H <sub>2</sub> SO <sub>4</sub>	− 0.44 (vs. SCE)	43	[33]
MoS <sub>2</sub> -PB/NG	GC	—	Drop-cast	0.5 M H <sub>2</sub> SO <sub>4</sub>	− 0.08 (vs. RHE)	62	[49]
MoS <sub>2</sub>	GC	0.24 mg cm <sup>-2</sup>	Drop-cast	0.1 M H <sub>2</sub> SO <sub>4</sub>	−0.117 (vs. RHE)	78	[24]
Ni-MoS <sub>2</sub>	CC	—	Chemical synthesis	1.0 M KOH	−0.098 (vs. RHE)	75	[43]
Ni-MoS <sub>2</sub>	CC	—	Chemical synthesis	0.5 M H <sub>2</sub> SO <sub>4</sub>	−0.110 (vs. RHE)	74	[43]
CuNi-P-MoS <sub>2</sub>	NFL	—	Chemical synthesis	0.5 M H <sub>2</sub> SO <sub>4</sub>	−0.225 (vs. RHE)	61	[2]
NiCo <sub>2</sub> S <sub>4</sub> /MoS <sub>2</sub>	NF	3.00 mg cm <sup>-2</sup>	Chemical synthesis	0.1 M KCl	−0.40 (vs. RHE)	—	[14]
MoS <sub>2</sub> -ZnO-Ni	NF	—	Chemical synthesis	1.0 M KOH	−0.129 (vs. RHE)	78	[45]
MoS <sub>2</sub> -NiS	GC	0.20 mg cm <sup>-2</sup>	Drop-cast	1.0 M KOH	−0.083 (vs. RHE)	66	[41]
DAC/MoS <sub>2</sub>	GC	2-5 mg cm <sup>-2</sup>	Drop-cast	0.5 M H <sub>2</sub> SO <sub>4</sub>	−0.090 (vs. RHE)	84	[36]
A-MoS <sub>2</sub>	GC	—	Drop-cast	2 M HNO <sub>3</sub>	−0.080 (vs. RHE)	97	[48]
RGO-MoS <sub>2</sub>	GC	—	Drop-cast	0.5 M H <sub>2</sub> SO <sub>4</sub>	−0.147 (vs. RHE)	36	[12]
RGO-MoS <sub>2</sub>	GC	20 μg	Drop-cast	0.5 M H <sub>2</sub> SO <sub>4</sub>	−0.130 (vs. RHE)	75	[27]
MoS <sub>2</sub> /MoSe <sub>2</sub>	CF	—	Chemical synthesis	0.5 M H <sub>2</sub> SO <sub>4</sub>	−0.162 (vs. RHE)	61	[22]
MoS <sub>2</sub>	GC	—	Drop-cast	0.5 M H <sub>2</sub> SO <sub>4</sub>	−0.185 (vs. RHE)	45	[42]
MoS <sub>2</sub>	GC	—	Drop-cast	0.5 M H <sub>2</sub> SO <sub>4</sub>	−0.230 (vs. RHE)	—	[30]
MoS <sub>2</sub> -g- CuNi <sub>2</sub> S <sub>4</sub>	SPE	0.30 mg cm <sup>-2</sup>	Drop-cast	0.5 M H <sub>2</sub> SO <sub>4</sub>	− 0.05 (vs. RHE)	29	This work

**Key:** CD/MoS<sub>2</sub>; carbon nanodot MoS<sub>2</sub> ensembles, GC; glassy carbon, —; no value given, RHE; reversible hydrogen electrode, P; phosphorus, NF; nickel foam, H; heteronanorods \*: produced by magnetron sputtering MoS<sub>2</sub> onto a nanocarbon substrate, SPE; screen-printed electrode, SCE; saturated calomel electrode, NC; nanocubes, MoS<sub>2</sub>-PB/NG; Fe<sub>4</sub>[Fe(CN)<sub>6</sub>]<sub>3</sub> NC with MoS<sub>2</sub> N-doped on graphene; CC; Carbon cloth, NFL; Nickel foil, DAC; Defective activated carbon A-MoS<sub>2</sub>; Acid engineered, RGO; Reduced graphene oxide, CF: Carbon fibre



**Table 2.** XPS elemental quantification of the CuNi<sub>2</sub>S<sub>4</sub>, g-CuNi<sub>2</sub>S<sub>4</sub>, MoS<sub>2</sub>-CuNi<sub>2</sub>S<sub>4</sub> and MoS<sub>2</sub>-g-CuNi<sub>2</sub>S<sub>4</sub> nanocomposites.

Element Composition (%)	CuNi <sub>2</sub> S <sub>4</sub>	g-CuNi <sub>2</sub> S <sub>4</sub>	MoS <sub>2</sub> -CuNi <sub>2</sub> S <sub>4</sub>	MoS <sub>2</sub> -g-CuNi <sub>2</sub> S <sub>4</sub>
Cu 2p <sub>3/2</sub>	3.14	2.33	2.06	2.72
Ni 2p <sub>3/2</sub>	5.72	5.37	4.11	4.41
O 1s	29.95	18.11	15.54	13.30
N 1s	7.88	3.97	2.73	4.28
C 1s	33.97	58.74	57.33	57.06
S 2p	19.33	11.48	15.95	17.04
Mo 3d	-	-	2.28	1.19

**Table 3.** XPS quantification of sulfur containing components of the CuNi<sub>2</sub>S<sub>4</sub>, g-CuNi<sub>2</sub>S<sub>4</sub>, MoS<sub>2</sub>-CuNi<sub>2</sub>S<sub>4</sub> and MoS<sub>2</sub>-g-CuNi<sub>2</sub>S<sub>4</sub> nanocomposites.

Sample	Atom % S	binding energy of 2p <sub>3</sub> (eV)	% of total S	atom %	Chemical state
CuNi <sub>2</sub> S <sub>4</sub>	19.33	161.1	36.69	7.09	metal-S
		162.5	22.12	4.28	metal bonded organic S <i>e.g.</i> metal-S-C
		164.6	5.89	1.14	organic S <i>e.g.</i> C-S
		168.5	35.3	6.82	sulfate, SO <sub>4</sub> <sup>2-</sup>
graphene-CuNi <sub>2</sub> S <sub>4</sub>	11.48	161.9	31.81	3.65	metal-S
		163.1	43.86	5.04	metal bonded organic S <i>e.g.</i> metal-S-C
		164.4	13.86	1.59	organic S <i>e.g.</i> C-S
		168.4	10.48	1.2	sulfate, SO <sub>4</sub> <sup>2-</sup>
MoS <sub>2</sub> -CuNi <sub>2</sub> S <sub>4</sub>	15.95	161.4	40.02	6.38	metal-S
		162.6	45.56	7.27	metal bonded organic S <i>e.g.</i> metal-S-C
		164.4	6.77	1.08	organic S <i>e.g.</i> C-S
		167.7	6.66	1.06	sulfate, SO <sub>4</sub> <sup>2-</sup>
MoS <sub>2</sub> -g-CuNi <sub>2</sub> S <sub>4</sub>	17.04	161.5	48.83	8.32	metal-S
		162.7	36.55	6.23	metal bonded organic S <i>e.g.</i> metal-S-C
		164.6	6.57	1.12	organic S <i>e.g.</i> C-S
		168.4	8.04	1.37	sulfate, SO <sub>4</sub> <sup>2-</sup>

**Figure 1.** Transmission electron microscopy (TEM)  $\text{MoS}_2$ -g- $\text{CuNi}_2\text{S}_4$  nanocomposite. Five sites of energy-dispersive X-ray (EDX) analysis are shown in (B) with the corresponding elemental compositions given in Table S1.

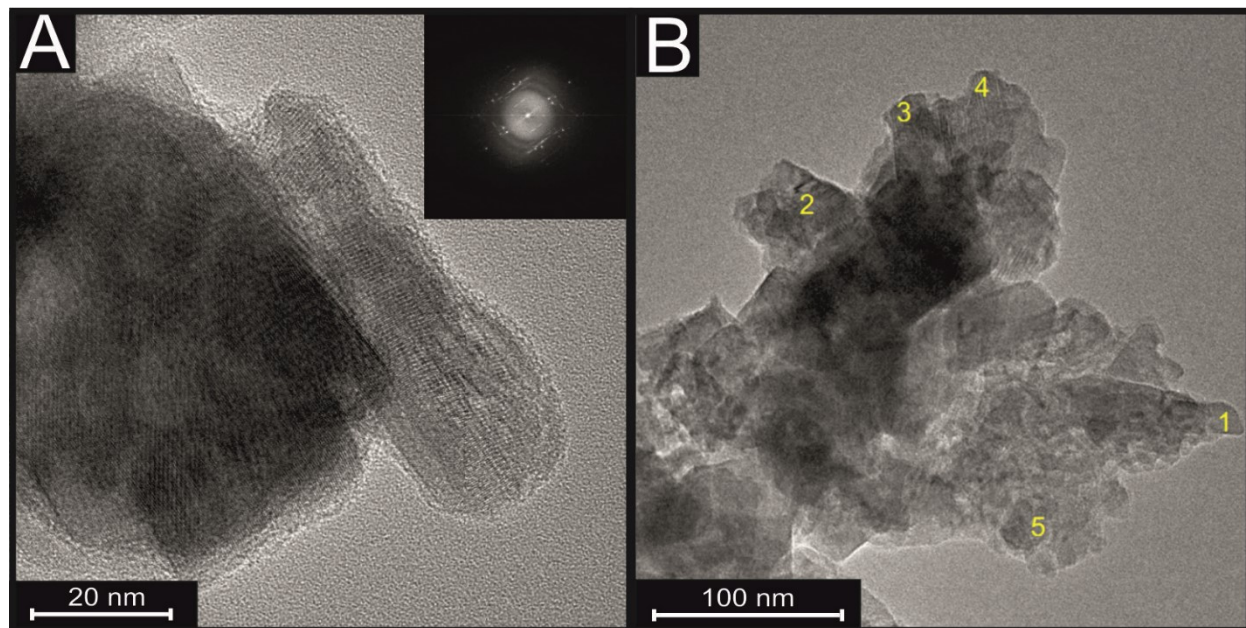


**Figure 2.** Physicochemical characterisation of the synthesized  $\text{MoS}_2$ -g- $\text{CuNi}_2\text{S}_4$  nanocomposites with FTIR (A), Raman (B), XPS (C) and XRD (D).

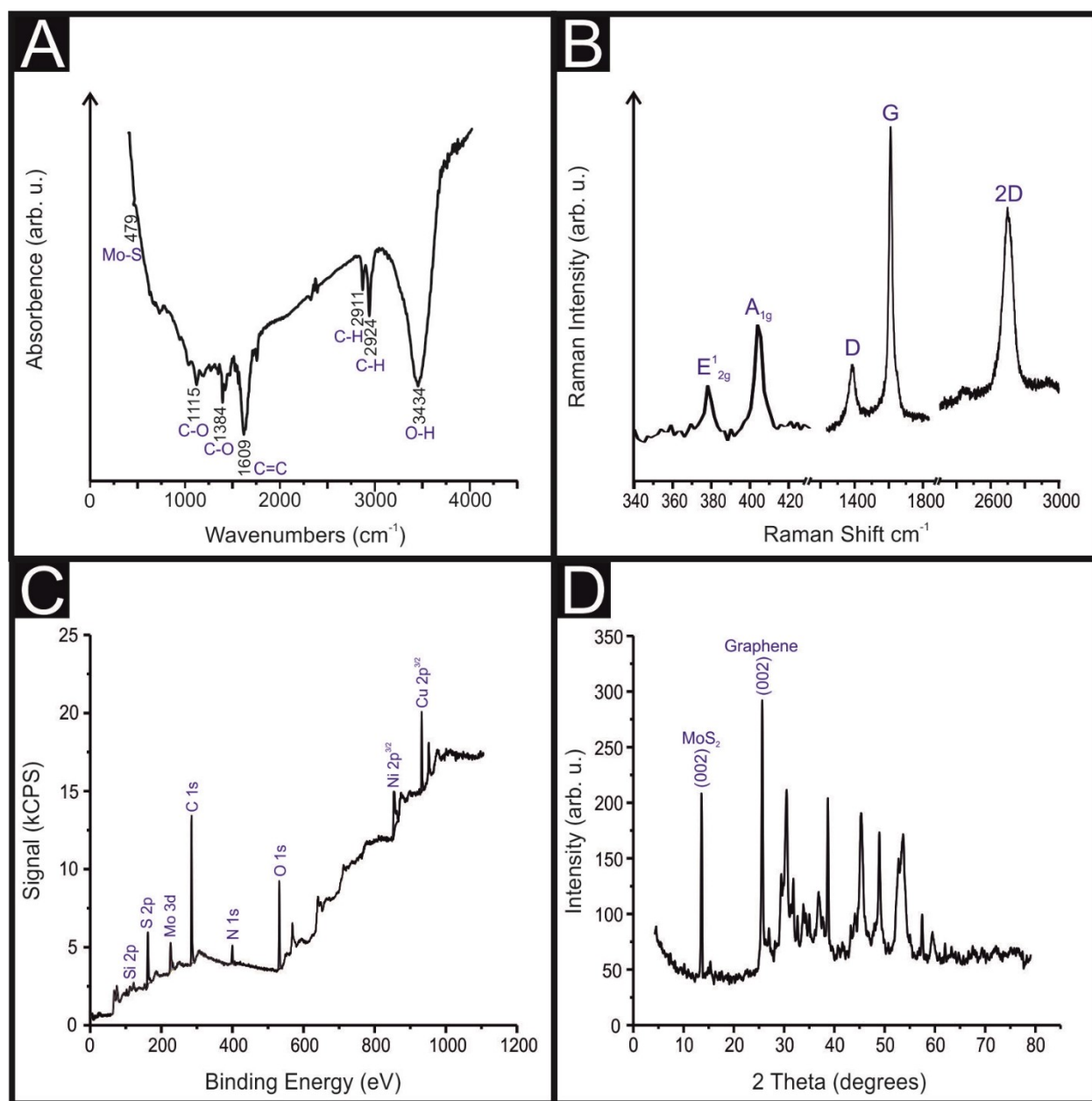
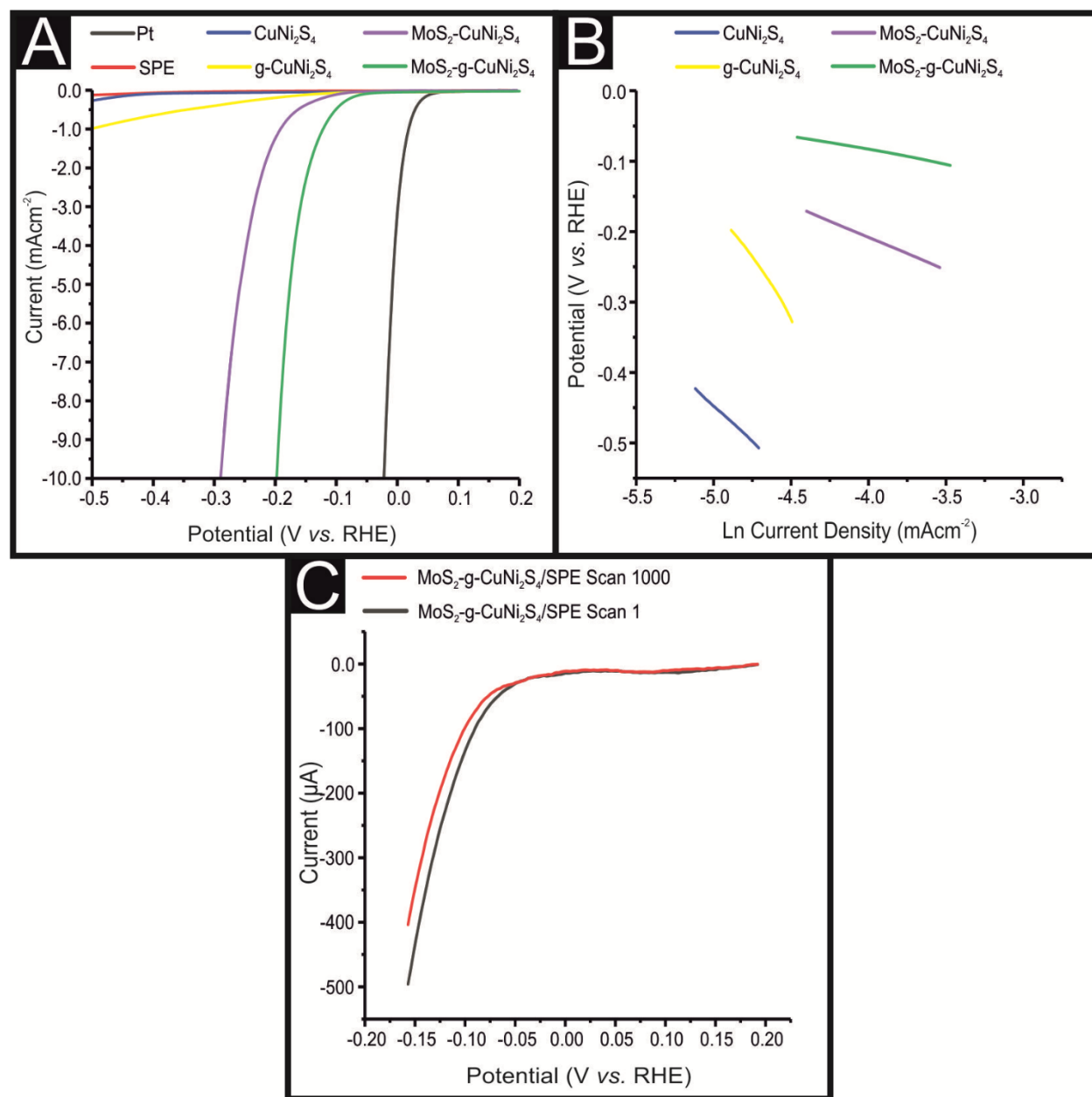


**Figure 3.** (A) Linear sweep voltammetry of unmodified and various modified electrodes showing HER activity of a bare/unmodified SPE, polycrystalline platinum electrode,  $\text{CuNi}_2\text{S}_4/\text{SPE}$ ,  $\text{g-CuNi}_2\text{S}_4/\text{SPE}$ ,  $\text{MoS}_2\text{-CuNi}_2\text{S}_4/\text{SPE}$  and  $\text{MoS}_2\text{-g-CuNi}_2\text{S}_4/\text{SPE}$ , Solution composition: 0.5 M  $\text{H}_2\text{SO}_4$ ; Scan rate:  $20 \text{ mVs}^{-1}$  (vs. RHE). (B) Tafel slopes corresponding to the Faradaic regions of the LSVs shown in (A). (C) Cyclic stability examination of a 10%  $\text{MoS}_2\text{-g-CuNi}_2\text{S}_4/\text{SPE}$  via LSV (scan rate:  $100 \text{ mV s}^{-1}$  (vs. RHE)) was performed between the potential range of 0 to  $-0.35 \text{ V}$ , repeated for 1000 cycles, this figure shows the first scan (black line), 1000<sup>th</sup> (red line).



## References

1. Ahmed A, Al-Amin AQ, Ambrose AF et al. (2016) Hydrogen Fuel and Transport System: A Sustainable and Environmental Future. *Int. J. Hydrogen Energy* 41:1369-1380
2. Ahn B-W, Kim T-Y, Kim S-H et al. (2018) Amorphous MoS<sub>2</sub> nanosheets grown on copper@nickel-phosphorous dendritic structures for hydrogen evolution reaction. *Appl. Surf. Sci.* 432:183-189
3. Benck JD, Chen Z, Kuritzky LY et al. (2012) Amorphous Molybdenum Sulfide Catalysts for Electrochemical Hydrogen Production: Insights into the Origin of their Catalytic Activity. *ACS Catal.* 2:1916-1923
4. Brownson DaC, Varey SA, Hussain F et al. (2013) Electrochemical properties of CVD grown pristine graphene: monolayer- vs. quasi-graphene. *Nanoscale* 6:1607-1621
5. Canton-Vitoria R, Vallan L, Urriolabeitia E et al. (2018) Electronic Interactions in Illuminated Carbon Dot/MoS<sub>2</sub> Ensembles and Electrocatalytic Activity towards Hydrogen Evolution. *Chem. Eur. J.* 24:10468-10474
6. Chou SS, Sai N, Lu P et al. (2015) Understanding catalysis in a multiphasic two-dimensional transition metal dichalcogenide. *Nat. Commun.* 6:8311
7. Escalera-López D, Niu Y, Yin J et al. (2016) Enhancement of the Hydrogen Evolution Reaction from Ni-MoS<sub>2</sub> Hybrid Nanoclusters. *ACS Catal.* 6:6008-6017
8. Ferrari AC (2007) Raman spectroscopy of graphene and graphite: Disorder, electron-phonon coupling, doping and nonadiabatic effects. *Solid State Commun.* 143:47-57
9. Foster CW, Kadara RO, Banks CE (2016) Screen-Printing Electrochemical Architectures. Springer International Publishing, Germany
10. Gong M, Li Y, Wang H et al. (2013) An Advanced Ni-Fe Layered Double Hydroxide Electrocatalyst for Water Oxidation. *J. Am. Chem. Soc.* 135:8452-8455
11. Görgün H (2006) Dynamic modelling of a proton exchange membrane (PEM) electrolyzer. *Int. J. Hydrogen Energy* 31:29-38
12. He HY, He Z, Shen Q (2018) Efficient hydrogen evolution catalytic activity of graphene/metallic MoS<sub>2</sub> nanosheet heterostructures synthesized by a one-step hydrothermal process. *Int. J. Hydrogen Energy*
13. Ji S, Yang Z, Zhang C et al. (2013) Exfoliated MoS<sub>2</sub> Nanosheets as Efficient Catalysts for Electrochemical Hydrogen Evolution. *Electrochim. Acta* 109:269-275
14. Jia Y, Ma Y, Lin Y et al. (2018) In-situ growth of hierarchical NiCo<sub>2</sub>S<sub>4</sub>/MoS<sub>2</sub> nanotube arrays with excellent electrochemical performance. *Electrochim. Acta* 289:39-46
15. Joensen PC, E. D. Alberding, N. Frindt, R. F. (1987) A Study of Single-Layer and Restacked MoS<sub>2</sub> by X-ray Diffraction and X-ray Absorption Spectroscopy. *J. Phys. C: Solid State Phys.* 20: 4043-4053
16. Kumar MP, Kesavan T, Kalita G et al. (2014) On the large capacitance of nitrogen doped graphene derived by a facile route. *RSC Adv.* 4:38689-38697
17. Lazar P, Otyepka M (2017) Role of the Edge Properties in the Hydrogen Evolution Reaction on MoS<sub>2</sub>. *Chemistry – A European Journal* 23:4863-4869
18. Lei Z, Xu S, Wu P (2016) Ultra-Thin and Porous MoSe<sub>2</sub> Nanosheets: Facile Preparation and Enhanced Electrocatalytic Activity Towards the Hydrogen Evolution Reaction. *Phys. Chem. Chem. Phys.* 18:70-74
19. Li G, Zhang D, Qiao Q et al. (2016) All The Catalytic Active Sites of MoS<sub>2</sub> for Hydrogen Evolution. *J. Am. Chem. Soc.* 138:16632–16638
20. Li H, Zhang Q, Yap CCR et al. (2012) From Bulk to Monolayer MoS<sub>2</sub>: Evolution of Raman Scattering. *Adv. Funct. Mater.* 22:1385-1390

21. Li P, Zeng HC (2017) Sandwich-Like Nanocomposite of CoNiOx/Reduced Graphene Oxide for Enhanced Electrocatalytic Water Oxidation. *Adv. Funct. Mater.* 27:1606325
22. Li S, Zang W, Liu X et al. (2018) Heterojunction engineering of MoSe<sub>2</sub>/MoS<sub>2</sub> with electronic modulation towards synergetic hydrogen evolution reaction and supercapacitance performance. *Open Chem. Eng. J.*
23. Li Y, Wang H, Xie L et al. (2011) MoS<sub>2</sub> Nanoparticles Grown on Graphene: An Advanced Catalyst for the Hydrogen Evolution Reaction. *J. Am. Chem. Soc.* 133:7296-7299
24. Li Z, Ma J, Zhou Y et al. (2018) Synthesis of sulfur-rich MoS<sub>2</sub> nanoflowers for enhanced hydrogen evolution reaction performance. *Electrochim. Acta* 283:306-312
25. Liu P, Zhu J, Zhang J et al. (2017) P Dopants Triggered New Basal Plane Active Sites and Enlarged Interlayer Spacing in MoS<sub>2</sub> Nanosheets toward Electrocatalytic Hydrogen Evolution. *ACS Energy Lett.* 2:745-752
26. Liu S, Zhang X, Shao H et al. (2012) Preparation of MoS<sub>2</sub> nanofibers by electrospinning. *Mater. Lett.* 73:223-225
27. Liu Y, Liu J, Li Z et al. (2018) Exfoliated MoS<sub>2</sub> with porous graphene nanosheets for enhanced electrochemical hydrogen evolution. *Int. J. Hydrogen Energy* 43:13946-13952
28. Naebe M, Wang J, Amini A et al. (2014) Mechanical Property and Structure of Covalent Functionalised Graphene/Epoxy Nanocomposites. *Sci. Rep.* 4:4375
29. Randviir EP, Brownson DaC, Metters JP et al. (2014) The fabrication, characterisation and electrochemical investigation of screen-printed graphene electrodes. *Phys. Chem. Chem. Phys.* 16:4598-4611
30. Ravikumar CH, Nair GV, Muralikrishna S et al. (2018) Nanoflower like structures of MoSe<sub>2</sub> and MoS<sub>2</sub> as efficient catalysts for hydrogen evolution. *Mater. Lett.* 220:133-135
31. Rowley-Neale SJ, Brownson DaC, Smith GC et al. (2015) 2D Nanosheet Molybdenum Disulphide (MoS<sub>2</sub>) Modified Electrodes Explored Towards the Hydrogen Evolution Reaction. *Nanoscale* 7:18152-18168
32. Rowley-Neale SJ, Foster CW, Smith GC et al. (2017) Mass-producible 2D-MoSe<sub>2</sub> bulk modified screen-printed electrodes provide significant electrocatalytic performances towards the hydrogen evolution reaction. *Sustainable Energy Fuels* 1:74-83
33. Rowley-Neale SJ, Ratova M, Fugita LTN et al. (2018) Magnetron Sputter-Coated Nanoparticle MoS<sub>2</sub> Supported on Nanocarbon: A Highly Efficient Electrocatalyst toward the Hydrogen Evolution Reaction. *ACS Omega* 3:7235-7242
34. Rowley-Neale SJ, Smith GC, Banks CE (2017) Mass-Produicable 2D-MoS<sub>2</sub>-Impregnated Screen-Printed Electrodes That Demonstrate Efficient Electrocatalysis toward the Oxygen Reduction Reaction. *ACS Appl. Mater. Interfaces* 9:22539-22548
35. Ruiz KH, Liu J, Tu R et al. (2018) Effect of microstructure on HER catalytic properties of MoS<sub>2</sub> vertically standing nanosheets. *J. Alloys Compd.* 747:100-108
36. Sangeetha DN, Selvakumar M (2018) Active-defective activated carbon/MoS<sub>2</sub> composites for supercapacitor and hydrogen evolution reactions. *Appl. Surf. Sci.* 453:132-140
37. Schultz MG, Diehl T, Brasseur GP et al. (2003) Air Pollution and Climate-Forcing Impacts of a Global Hydrogen Economy. *Science* 302:624-627
38. Shi Y, Zhou Y, Yang D-R et al. (2017) Energy Level Engineering of MoS<sub>2</sub> by Transition-Metal Doping for Accelerating Hydrogen Evolution Reaction. *J. Am. Chem. Soc.* 139:15479-15485
39. Shin S, Jin Z, Kwon DH et al. (2015) High Turnover Frequency of Hydrogen Evolution Reaction on Amorphous MoS<sub>2</sub> Thin Film Directly Grown by Atomic Layer Deposition. *Langmuir* 31:1196-1202
40. Sudesh, Kumar N, Das S et al. (2013) Effect of graphene oxide doping on superconducting properties of bulk MgB<sub>2</sub>. *Supercond. Sci. Technol.* 26:095008

41. Tang C, Zhang H, Xu K et al. (2018) Scalable synthesis of heterostructure molybdenum and nickel sulfides nanosheets for efficient hydrogen generation in alkaline electrolyte. *Catal. Today* 316:171-176
42. Wan Y, Zhang Z, Xu X et al. (2018) Engineering active edge sites of fractal-shaped single-layer MoS<sub>2</sub> catalysts for high-efficiency hydrogen evolution. *Nano Energy* 51:786-792
43. Wang Q, Zhao ZL, Dong S et al. (2018) Design of active nickel single-atom decorated MoS<sub>2</sub> as a pH-universal catalyst for hydrogen evolution reaction. *Nano Energy* 53:458-467
44. Wang T, Liu L, Zhu Z et al. (2013) Enhanced electrocatalytic activity for hydrogen evolution reaction from self-assembled monodispersed molybdenum sulfide nanoparticles on an Au electrode. *Energy Environ. Sci.* 6:625-633
45. Xu L, Wang S (2018) A novel hierarchical MoS<sub>2</sub>-ZnO-Ni electrocatalyst prepared by electrodeposition coupling with dealloying for hydrogen evolution reaction. *J. Electroanal. Chem.* 808:173-179
46. Yang Y, Zhang K, Lin H et al. (2017) MoS<sub>2</sub>-Ni<sub>3</sub>S<sub>2</sub> Heteronanorods as Efficient and Stable Bifunctional Electrocatalysts for Overall Water Splitting. *ACS Catal.* 7:2357-2366
47. Zhang J, Wu J, Guo H et al. (2017) Unveiling Active Sites for the Hydrogen Evolution Reaction on Monolayer MoS<sub>2</sub>. *Adv. Mater.* 29:1701955
48. Zhang W, Xie Z, Wu X et al. (2018) Acid-engineered defective MoS<sub>2</sub> as an efficient electrocatalyst for hydrogen evolution reaction. *Mater. Lett.* 230:232-235
49. Zhang X, Wu Y, Sun Y et al. (2018) Hybrid of Fe<sub>4</sub>[Fe(CN)<sub>6</sub>]<sub>3</sub> nanocubes and MoS<sub>2</sub> nanosheets on nitrogen-doped graphene realizing improved electrochemical hydrogen production. *Electrochim. Acta* 263:140-146
50. Zhao J, Zhang Z, Yang S et al. (2013) Facile synthesis of MoS<sub>2</sub> nanosheet-silver nanoparticles composite for surface enhanced Raman scattering and electrochemical activity. *J. Alloys Compd.* 559:87-91